X-ray conversion of ultra-short laser pulses on a solid sample: Role of electron waves excited in the pre-plasma

F. Baffigi, G. Cristoforetti, L. Fulgentini, A. Giulietti, P. Koester, L. Labate, and L. A. Gizzi

Citation: Physics of Plasmas (1994-present) **21**, 072108 (2014); doi: 10.1063/1.4886977
View online: http://dx.doi.org/10.1063/1.4886977
View Table of Contents: http://scitation.aip.org/content/aip/journal/pop/21/7?ver=pdfcov
Published by the AIP Publishing

X-ray conversion of ultra-short laser pulses on a solid sample: Role of electron waves excited in the pre-plasma

F. Baffigi,[a] G. Cristoforetti, L. Fulgentini, A. Giulietti, P. Koester, L. Labate, and L. A. Gizzi
Intense Laser Irradiation Laboratory, Istituto Nazionale di Ottica, CNR Campus, Via G. Moruzzi 1, 56124, Pisa, Italy

(Received 25 February 2014; accepted 23 June 2014; published online 7 July 2014)

Flat silicon samples were irradiated with 40 fs, 800 nm laser pulses at an intensity at the best focus of $2{\cdot}10^{18}$ Wcm^{-2}, in the presence of a pre-plasma on the sample surface. X-ray emission in the spectral range from 2 to 30 keV was detected inside and outside the plane of incidence, while varying pre-plasma scale length, laser intensity, and polarization. The simultaneous detection of 2ω and $3\omega/2$ emission allowed the contributions to the X-ray yield to be identified as originating from laser interaction with either the near-critical density (n_c) region or with the $n_c/4$ region. In the presence of a moderate pre-plasma, our measurements reveal that, provided the pre-plasma reaches a scale-length of a few laser wavelengths, X-ray emission is dominated by the contribution from the interaction with the under dense plasma, where electron plasma waves can grow, via laser stimulated instabilities, and, in turn, accelerate free electrons to high energies. This mechanism leads also to a clear anisotropy in the angular distribution of the X-ray emission. Our findings can lead to an enhancement of the conversion efficiency of ultra short laser pulses into X-rays. © *2014 AIP Publishing LLC*. [http://dx.doi.org/10.1063/1.4886977]

I. INTRODUCTION

Irradiation of solid samples with ultra-short (<100 fs) intense (>10^{16} W/cm^2) laser pulses is an efficient way to convert laser light into X-rays.[1] Various physical processes are involved in the overall conversion: their comprehension, still not complete, needs a detailed knowledge of the interaction parameters. In particular, it is well known that the laser pulse contrast (ratio between the main pulse peak power and the power delivered by the "pre-pulse" emission) plays a decisive role in setting the regime of interaction, via interplay between several phenomena. In fact, the early action of the pre-pulse on the sample produces a "pre-plasma" which screens the solid surface and prevents it from direct laser irradiation. This kind of effect is almost unavoidable but its actual relevance on the processes involved in the laser conversion into X-rays depends on pre-plasma parameters. If the pre-plasma thickness above the solid surface is very small, the X-ray conversion is mostly due to phenomena starting from laser absorption close to the critical density n_c ($n_c = 1.1{\cdot}10^{21}/\lambda_0{}^2$, where λ_0 is the laser wavelength expressed in μm), including generation of supra-thermal electrons. Such energetic electrons can in turn transport energy into the overcritical region and deliver it to the solid. When the density scale length becomes much shorter than λ_0, the absorption occurs properly at or very close to the solid surface, within a skin depth.[2] This extreme condition is not the subject of our measurements. If, instead, the pre-plasma extension, namely the scale-length of the under-dense region, becomes important (a few laser wavelength or more) the laser-plasma coupling can trigger a series of processes including laser-driven plasma instabilities. These processes compete with the laser-plasma interaction near the critical density layer and can change the balance between the various contributions to the X-ray conversion. Particularly relevant to this scenario is the influence of laser polarization on the possibility that laser light could excite electron plasma waves (EPW) of large amplitude which, in turn, can accelerate a fraction of the available free electron population to high kinetic energies, leading to X-ray emission via Bremsstrahlung. In the case of P-polarization, laser light couples more efficiently with the critical density region. So, even small scale-lengths can support laser energy absorption via Resonance Absorption or Brunel process.[3,4] In contrast, S-polarized light is highly reflected by the plasma region near n_c, with reduced energy deposition near the critical density, but enhanced possibility of exciting plasma instabilities also with the contribution of the reflected light, provided the plasma has a suitable scale-lengths in the under-dense region.[5,6]

Historically, all the nonlinear effects related to the laser-plasma coupling, in particular all the parametric stimulated instabilities, including SRS (Stimulated Raman Scattering) and TPD (Two Plasmon decay), were investigated in detail in the long pulse regime (pulse duration longer than 100 ps),[7–9] during the 1980s and 1990s, in the framework of the Inertial Confinement Fusion (ICF).[10] In some cases, these studies were aimed at characterizing X-ray sources[11] and study hot electron generation.[12,13] However, little information on the role of polarization emerged from these studies, due to the long pre-plasma, which prevented significant interaction at the critical density. Moreover, with ultra-short pulses, the pre-plasma scale length and the conditions for the growing of the instabilities are very different.

In the case of short pulse, at sub-relativistic intensities and in the presence of a significant pre-pulse, as in Ref. 14, a strong 2ω emission and strong backscattering radiation were observed for I > 10^{15} W/cm^2. Soom *et al.*[15] found a strong Kα emission, mainly induced by hot electrons, at the intensity of $4{\cdot}10^{15}$ W/cm^2, with a laser of 1 μm wavelength and 1

[a]federica.baffigi@ino.it. URL: www.ino.it.

ps pulse, like in the experiment of Ref. 13. Moreover, they found that the strong dependence of the Kα emission on the angle of the incidence and polarization of laser light was consistent with hot electrons generated by resonance absorption. In fact, the X-ray signal was found to be maximum with P-polarized laser light and that was a clear indication of Resonance Absorption (RA) at near-critical plasma density. On the contrary, Chaker *et al.*[14] did not observe any dependence of the Kα emission on the laser light polarization and attributed this finding to surface rippling in the preformed plasma. Numerical simulations, carried out with and without a pre-pulse, supported this conclusion. On the other hand, parametric instabilities were also found to play a role in X-rays generation by laser irradiation of solid targets with ultra-short pulses at relativistic intensities[16,17] where, in principle, laser polarization is expected to play a role. Also in these conditions, the role of pre-pulse was highlighted, at similar intensities, for example, in Refs. 18 and 19, as useful tool for improving X-ray emission.

Interestingly, in the relativistic regime ($a_0 \geq 1$, where $a_0 = 8.53 \cdot 10^{-10}\ (I\lambda_0^2)^{1/2}$, with I and λ_0 expressed, respectively, in W/cm^2 and μm, represents the normalized laser field amplitude), measurements of the X-rays yield and simultaneously of the second harmonic emission, often reveal anti-correlation. This is mostly due to the development of an optimum density scale length of the plasma near the critical density[20] or, in the case of P polarized laser light, to the occurrence of matched conditions for the resonance absorption[21] or Brunel mechanism. As for three-halves harmonic ($3\omega/2$) emission, mainly due to (TPD), it requires suitable density scale-length in the region around $n_c/4$. This requirement basically remains valid with ultra-short and ultra-intense pulses, but the higher laser intensities generally result in a significant reduction of the scale length needed for the growth of the TPD instability.[22–25]

The formation of a pre-plasma can provide, before of the arrival of the main pulse, a scale length suitable for stimulated instabilities to grow. Veisz *et al.*[26] reported the first measurements of $3\omega/2$ emission in a long density scale-length plasma ($L \approx 100/200\ \lambda_0$) in the ultra-short pulse regime (100 fs). Furthermore, the same group[22] carried out a detailed theoretical study on the TPD instabilities and reported experimental measurements of the angular distribution of $3\omega/2$ emission from fs laser pulse at higher intensity (up to $6 \cdot 10^{18}$ W/cm^2). With this intensity, a much shorter density scale length was enough for observing three-halves harmonic emission. Similar results were previously achieved by Tarasevitch *et al.*,[23] who observed $3\omega/2$ emission at extremely short plasma scale lengths ($L \approx \lambda_0$) for a peak intensity of $7 \cdot 10^{17}$ W/cm^2. In this case, the excited plasma waves had a very broad spectrum and the $3\omega/2$ emission was highly collimated. A distinctive feature of these studies was the directionality of the X-ray emission, which was found to be strictly correlated to the directionality of the $3\omega/2$ emission.[22,23] The latter was proven to be maximum in the plane of incidence for P-polarization and in the perpendicular plane for S-polarization.[12,22]

Non-isotropic distribution of the X-ray yield was further investigated by different authors.[12,17] In Ref. 12, the hot electron energy distribution was measured at various angles, with a CO_2 laser beam ($\lambda_0 = 10.6\ \mu$m, $\tau = 20$ ns and $I = 4 \cdot 10^{14}$ W/cm^2), showing that the hot electron emission is maximum at about 45° with respect to the **k** vector of the incident beam, both in the forward and backward directions, in the plane of polarization of the incident beam. Chen *et al.*[17] reported the angular distribution of the hot electrons, but at intensities from 10^{17} to 10^{19} W/cm^2 and pulse duration from 70 to 400 fs. Other authors[22,23] reported detailed measurements of the angular distribution of $3\omega/2$ radiation. Soom *et al.*[15] mentioned a strong polarization dependence of the X-ray emission. In particular, they found the maximum X-rays emission for P-polarized light at an angle of incidence of around 50°, while for S-polarized laser light, the maximum x-ray emission is observed at perpendicular incidence.

Our aim is to investigate the role of laser-driven instabilities in presence of a pre-plasma and to identify the role of laser polarization, also in view of an efficient X-ray emission On the other hand, we were not interested at investigating the absolute performances laser-driven secondary sources of X-rays with different samples including high Z materials, as it is the case of Ref. 16. Our experimental campaign, instead, was devoted at evaluate the laser-to-X-ray conversion efficiency by using silicon samples, with different structures on their surface, using a flat silicon sample as reference. Since flat silicon samples gave interesting results by themselves, this paper is focused on these ones. The results obtained by using silicon targets with nanostructures on their surface are reported in Ref. 27.

Here, in particular, we clarify the role of instabilities in presence of preplasma. In fact, we focus on the balance of different contributions to the non-thermal X-ray conversion of the laser energy, either by interaction with the near-critical region and/or by interaction with the under-dense region, and for S and P polarizations. To this purpose, amplified spontaneous emission (ASE) from the laser system is used to heat the target for a few nanosecond before the arrival of the main pulse. The X-ray yield was measured by two different detectors placed at different viewing directions. Second harmonic generation was monitored as a marker of the laser coupling at the critical density n_c. Three half harmonic generation was instead used as the marker of laser coupling at $n_c/4$, where Two Plasmons Decay and/or Stimulated Raman Scattering instabilities[5,6] take place. Our measurements show a clear evidence of the strong correlation between the directionality of X-ray emission and the behavior of the $3\omega/2$ emission, this latter originating from the development of suitable pre plasma scale-length.

The paper is organized as follows. After the introduction, in Sec. II, the experiment is described in detail. In Sec. III, the results are presented, together with data from hydrodynamic simulations of the pre-formed plasma. Section IV is devoted to a general discussion of the physical scenario revealed by our experiment. Finally, the main conclusions are summarized in Sec. V.

II. THE EXPERIMENT

The experiment was carried out using the multi-TW, Ti:Sapphire laser at ILIL lab, CNR Campus, Pisa (Italy). The

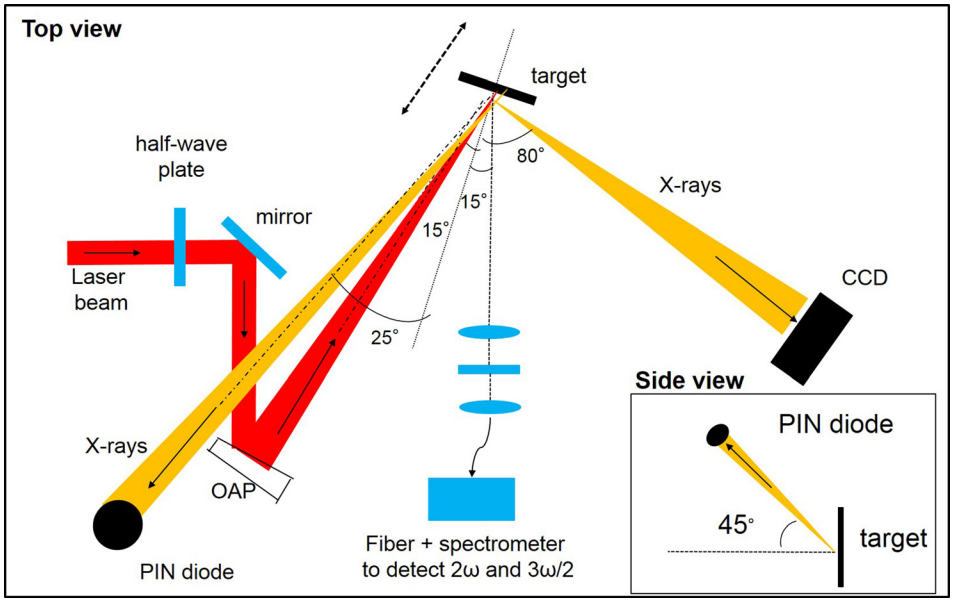

FIG. 1. Geometry of irradiation and detection.

laser, based on the CPA (Chirped Pulse Amplification) technique, operates at a fundamental frequency of 792 nm and for this experiment delivered 2-TW, 40 fs pulses. The measured beam quality parameter M^2 was ~1.7 and the contrast at 1 ns before the main peak was $2.5 \cdot 10^7$. The nanosecond pre-pulse was due to Amplified Spontaneous Emission (ASE), whose duration was about 3 ns (FWHM). A focal spot of 7 μm (FWHM) was produced by a f/5 off axis parabola (OAP). Laser intensity at best focus was then $I \approx 2.5 \cdot 10^{18}$ Wcm^{-2}.

The normalized laser field amplitude a_0 was ~1, corresponding to a moderately relativistic laser intensity. The laser was focused on a flat silicon target, mounted on a motorized three-axis translational stage, to ensure that fresh target portions were exposed to each laser irradiation. The target was irradiated at an angle of incidence of 15° (Fig. 1) in a vacuum chamber, whose residual pressure was 10^{-4} mbar. X-rays emitted by the plasma were collected by two detectors, looking from two different directions, to investigate non-isotropic effects in X-ray emission. A PIN diode was placed at an angle of 45° with respect to the horizontal plane of incidence (Fig. 1). A back-illuminated cooled CCD camera (Princeton Instruments), working in single-photon regime,[28] was located in the plane of incidence at a large angle (≈80°) with respect to the target normal. In front of the CCD aluminum and Mylar foils were used as attenuators, in order to keep the single-photon regime of detection. The peak of sensitivity of the PIN and of the CCD is located around 6 and 5 keV, respectively. For both detectors, the sensitivity drops down to about 10% of the maximum at 2 keV towards low energy and 30 keV towards high energy, respectively. Both soft and hard components of the emitted X-ray spectrum were partially included in this range. The visible light emitted in the specular direction to the incident laser light was collected by an optical system in a cone with the opening angle of 20° and injected into a fiber spectrometer. Optical spectra thus obtained ranged from 210 nm to 850 nm and included both the 2ω and $3\omega/2$ harmonics of the laser light, with a spectral resolution of around 1 nm (see Fig. 3(b)). Two different series of measurements were performed. In one series, measurements were carried out (either with P- or S-polarized laser light) by moving the target along the axis of the laser propagation, with steps of 50 μm. This allowed us to vary simultaneously the laser intensity and pre-plasma scale-length. In the other series, a motorized half wave plate (suitable for the 0.792 μm wavelength at high intensity) was placed before the entrance of the vacuum chamber (Fig. 1), in order to gradually vary the polarization of the laser light from P to S.

III. EXPERIMENTAL AND NUMERICAL RESULTS

The set-up shown in Fig. 1 was used to measure the X-ray yield in different conditions of laser light (intensity and polarization) and pre-formed plasma parameters. Sets of measurements were taken varying the polarization of the laser light by rotating a half wave-plate, step by step, from P to S. Preliminarily, a set of measurements was taken performing a focal scan. This resulted in the variation of the intensity of both main pulse and ASE onto the target. The change of ASE irradiance, in turn, results in the variation of pre-plasma parameters (in particular of its density scale length).

A. 2ω, $3\omega/2$, and X-rays vs. sample position (focal scan) with P-polarized laser light

Figs. 2 and 3 show the results of the focal scan in P-polarization. The plot in Fig. 2 compares the intensity of X-rays, detected both by PIN diode and CCD, vs. position, while the plot in Fig. 3(a) compares the intensity of 2ω and $3\omega/2$ vs. position. Data were obtained by moving the target along the laser axis (z axis) with steps of 50 μm. Intensity is expressed in arbitrary units for each of the four quantities The points indicated as "X-PIN" represent the peak values of the signal of the PIN diode, whereas the points indicated as "X-CCD" give the X-ray flux values obtained by integrating the active area of CCD camera, after the subtraction of the background signal.[28] We performed a focal scan in both

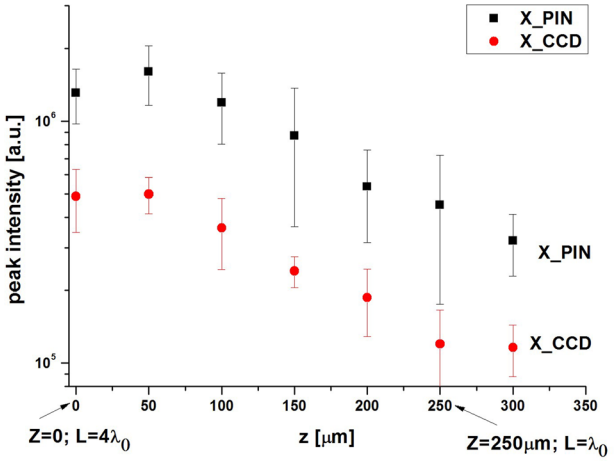

FIG. 2. Focal scan in P-polarization, showing the intensity of X-rays, detected by the PIN and CCD, vs. target position (z axis). The plasma scale length L at quarter-critical density, calculated from numerical simulations, is also indicated at two positions, $Z = 0$ and $Z = 250\ \mu$m, respectively.

direction, $Z > 0$ and $Z < 0$, finding a strong symmetry in the trends of "X_PIN," "X_CCD" 2ω and $3\omega/2$ signals. Thanks to this symmetry, we opted for representing these two trends just as a single direction $Z > 0$, starting from $Z = 0$, which corresponds to the best focal position. Actually, we considered the **absolute value** of Z. So, each point corresponding to a given z in the graph of Fig. 2 is the average value between the values obtained at $Z = \mathbf{z}$ and $Z = -\mathbf{z}$. In this way, each point in the plot is obtained from eight single measurements and is reported with its variance bar. We choose this representation also for the focal scan in p-polarization with the measurements of 2ω and $3\omega/2$ in (Fig. 3), and the focal scan in s-polarization (Fig. 7).

As expected, the X-ray intensity (Fig. 2) depends strongly on the target position and exhibits a maximum around the best-focus position, the same position where $3\omega/2$ also has a maximum and 2ω has a minimum (Fig. 3(a)). The 3/2 harmonic emission vanishes for target positions approximately 300 μm away from the best focus. Figures 3(b) and 3(c) show the optical spectra in a spectral region including the second and the three half harmonic. The spectrum in Fig. 3(b) is taken at $Z = 0$. Conversely, the spectrum in Fig. 3(c) is referred to $Z = 300\ \mu$m where the $3\omega/2$ is below detection and the 2ω reaches its peak intensity. The two spectra are integrated over four shots. Interestingly, in spite of the integration over many shots, the multi-peaked modulations of both 2ω and $3\omega/2$ are visible. This confirms that the spectral

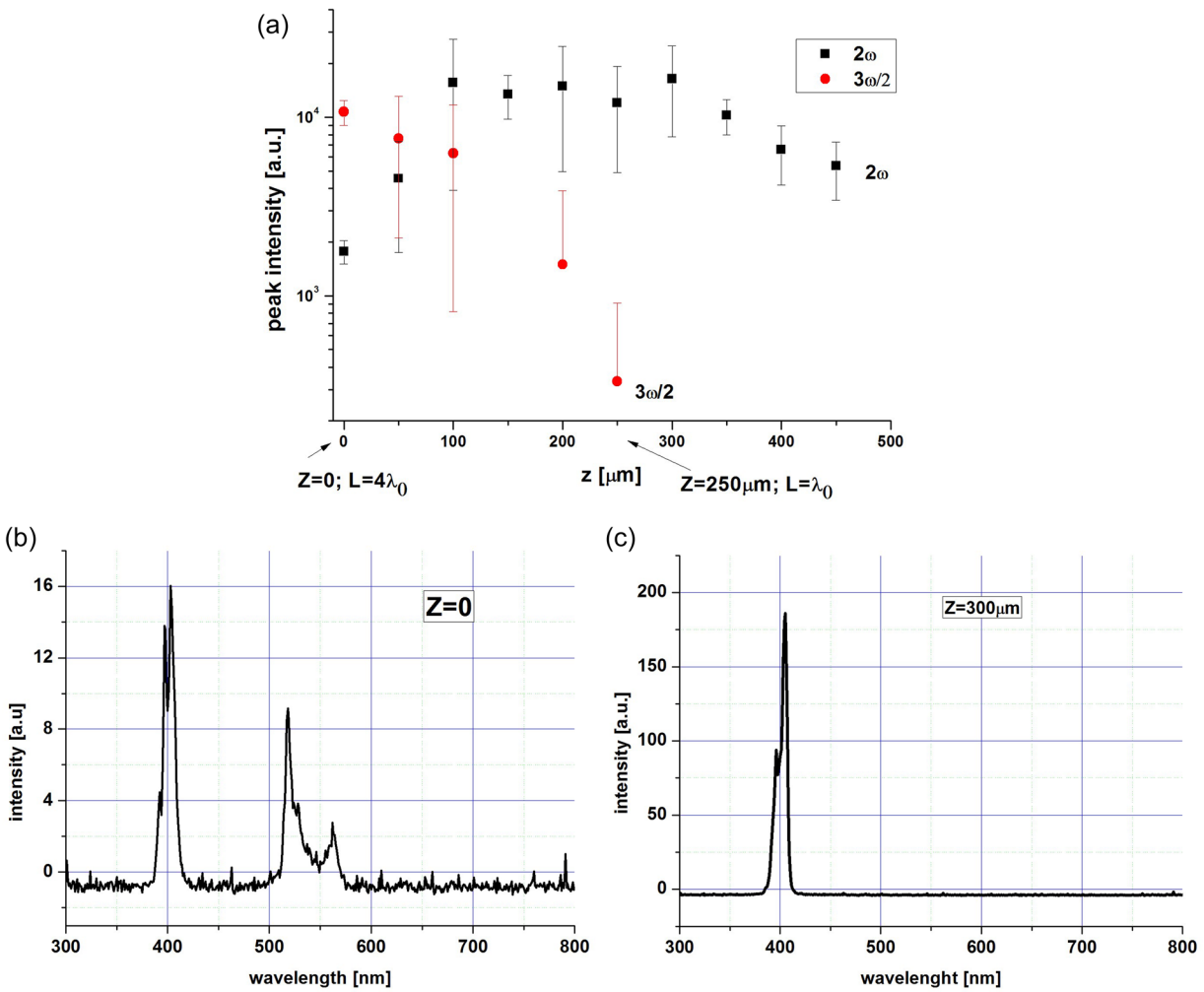

FIG. 3. (a) Focal scan in P-polarization, showing the intensity of 2ω and $3\omega/2$ vs. target position (z axis). The plasma scale length L at quarter-critical density, calculated from numerical simulations, is also indicated at two positions, $Z = 0$ and $Z = 250\ \mu$m, respectively.(b) Optical spectrum at $Z = 0$. (c) Optical spectrum at $Z = 300\ \mu$m.

features observed here are reproducible from shot to shot. In fact, the spectral modulations were observed in all the spectra independently from the sample position together with a broadening around the nominal values of $\lambda = 396$ nm for 2ω and $\lambda = 528$ nm for $3\omega/2$, respectively.

Indeed, the occurrence of $3\omega/2$ emission in the proximity of the best focus, as from Fig. 3(a) is a clear evidence of a pre-plasma whose scale-length, at the arrival of the main pulse, allows some instabilities to grow, including Two-Plasmon Decay and maybe Stimulated Raman Scattering around the $n_c/4$ region. In fact, at the best focus position the ASE intensity is also maximum and pre-plasma formation occurs early during the interaction. Moving the target away from this best position makes the ASE intensity on target decrease progressively until the pre-plasma scale-length, at the arrival of the main pulse, becomes too short to activate any instability.

The pre-plasma scale length region at $n_c/4$ density was estimated using the 2D Eulerian hydrodynamic code POLLUX (see Ref. 29, for more details), which includes laser absorption via inverse Bremsstrahlung and thermal electron transport via flux-limited Spitzer-Harm conductivity. A 3 ns FWHM Gaussian ASE pedestal, at different intensities onto the target, was considered. The simulation time was 6 ns, with 4 ns between the run starting point and the pedestal peak (which corresponds also to the arrival of the main pulse). Assuming a constant ratio between the ASE and the main pulse peak intensity, we calculated the values of the intensities of the ASE pulse for each Z position. In this way, we find that the ASE intensity ranges from $1 \cdot 10^{11}$ W/cm^2 ($Z = 0$) to $1.3 \cdot 10^{10}$ W/cm^2 ($Z = 300\ \mu$m, which correspond to the first focal position where the $3\omega/2$ disappears in P-polarization). From simulation data, we find that the ASE at the best focus position produces a plasma, whose density scale-length at $n_c/4$ is about $L_{(nc/4)} \approx 4\lambda_0$ at the arrival of the main pulse. Differently, in the plasma produced by the ASE when target is around 250 μm away from best focus, $L_{(nc/4)}$ is approximately equal to λ_0. The Rayleigh length of the pulse was around 100 μm. Data shown in Fig. 3(a) show that this is the smaller possible scale length to observe $3\omega/2$ in our conditions. It has to be noticed[22–24] that the intensity of the main pulse at that target position, namely $I \approx 4.5 \cdot 10^{17}$ Wcm^{-2} would be still enough to excite TPD provided a suitable plasma scale-length exists. Therefore, while the maximum X-ray yield appears to be a combined effect of both maximum intensities of main pulse and ASE, the vanishing of $3\omega/2$ emission is mostly likely due to the lower plasma scale length. In other words, the maximum X-ray conversion occurs when the intense pulse propagates through a well-developed plasma in front of the solid target. During the laser propagation through the $n_c/4$ region.[8,9,22] TPD occurs with the generation of plasma waves at $\omega/2$, that subsequently can combine with ω photons and generate the $3\omega/2$ emission. As presented below, vectorial calculations in the wave vector space show that, in our experimental setup, the TPD plasmons can easily mix with laser photons and generate $3\omega/2$ emission.[22] The process also appears to be favored by the fact that no propagation of the plasmon is needed to allow the phase matching between plasmon and laser photon. Conversely, calculations show that SRS can also contribute to $3\omega/2$, but the phase matching requires plasma waves produced at densities $n_e < 0.19 n_c$ and is favoured by plasmon propagation in the under-dense plasma. Our attention here is mainly focused on the TPD process, whose occurrence is suggested by the X-ray emission results. However, a possible occurrence of SRS does not change the argument we use for explaining the X-ray correlation with $3\omega/2$. Such correlation suggests that plasma waves growth and subsequent wave breaking lead to the ejection of supra-thermal electrons, and consequently, via *Bremsstrahlung*, to the emission of hard X-rays.

Figure 3(a) also shows that second harmonics is minimum at "best focus for X-rays" ($Z = 0$). This could be caused by the relatively long scale-length plasma in front of the target, which results in the absorption of part of the laser energy by TPD and SRS instabilities and prevents a significant portion of the laser light from reaching regions close to the critical density n_c, where the 2ω generation occurs. Differently, 2nd harmonic generation exhibits a broad maximum for target positions between $Z = 100\ \mu$m and $Z = 300\ \mu$m, in spite of the decreased intensity of the main pulse at those positions. This maximum occurs at a position where a trade-off exists between a sufficiently steep density profile and a sufficiently high laser intensity. Indeed, the steepness of the density gradient is a dominant factor in the 2ω generation because of the non-linearity of the process. As further discussed below, this feature is enhanced with P-polarized laser light as observed in a previous experiment.[21]

B. 2ω, $3\omega/2$, and X-rays vs. polarization at maximum laser intensity

A polarization scan was carried out with the target placed in the best focus position for P-polarization ($Z = 0$), and the polarization of laser radiation was progressively rotated from P to S, by means of a motorized half-wave plate. Figure 4 shows the variations of 2ω and $3\omega/2$, while Figure 6 shows the variation of X-ray intensity (collected by PIN diode and CCD, respectively), versus polarization of the laser pulse. The dotted lines in each figures represent the detection threshold. Each point in Figures 4 and 6 is the

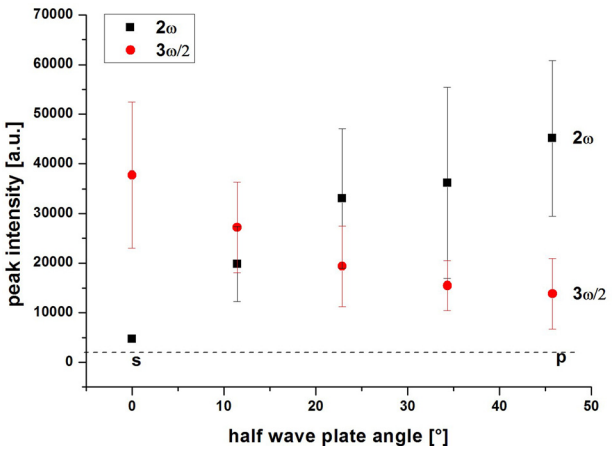

FIG. 4. 2ω and $3\omega/2$ yield vs. the half wave plate angular position, changing the laser polarization from S to P.

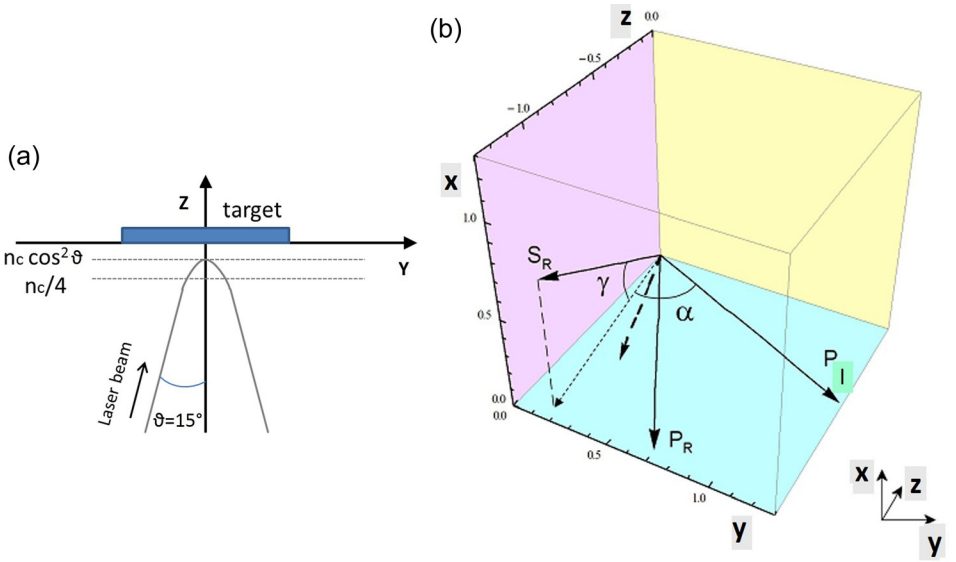

FIG. 5. (a) Geometry of laser propagation in the x-y plane; (b) Wave vectors of $3/2\omega$ photons (normalized to c/ω_0) produced by a TPD-induced plasmon in case of *p* and *s* polarized laser beams. P_R and P_I indicate the wave vectors produced in *p*-beam irradiation by coupling of TPD plasmons with reflected and incident laser photons. Similarly, S_R indicates the wave vector produced in s-beam irradiation by the coupling of a TPD plasmon with a reflected photons. The dashed arrow indicates the direction of the reflected beam, forming an angle ϑ of 15° with respect to the target normal.

average value of the peak intensity, while the points indicated as "X_CCD" in Fig. 6 represent the X-rays detected by the CCD, namely flux values, obtained integrating the images taken with the CCD. Both are calculated over a number of shots, typically 8, which correspond to four shots for each position both for $Z > 0$ and $Z < 0$, and reported with their variance bar, as explained in the previous Section.

As expected, 2ω generation (Fig. 4) decreases considerably (about one order of magnitude) by changing laser light polarization from P to S, because of the weaker coupling of S-polarized laser light with the layers near n_c. An opposite behavior is shown for $3\omega/2$ generation (Fig. 4), showing an increased coupling of S-polarized light with the under-dense plasma and, in particular, around $n_c/4$. In fact, a stronger reflected beam occurs in S-polarization, due to the less efficient absorption at the critical density. Since the $3\omega/2$ emission can be produced both by the incident and reflected beam, the S-polarized light is expected to generate a stronger $3\omega/2$ emission (about a factor 5 compared to P polarization), due to the significantly larger intensity of the reflected beam.

According to theory, angular distribution of $3\omega/2$ emission depends upon phase matching conditions. These conditions in some cases are not satisfied directly in the region where the plasmons are produced, but after the propagation of the plasmons in the underdense plasma region. Considering the non isotropic behavior of plasmon generation by TPD, different directions of $3/2\omega$ wave vectors $k_{3/2}$ are expected for different laser beam polarizations. Finally, it is worth taking into account that the plasma wave can couple both with the incoming laser photons (direct coupling) and with the photons reflected by the critical surface (reflection coupling). Fig. 5(a) represents schematically the geometry of laser propagation in the y-z plane. Figure 5(b) reports the calculated wave vectors of $3/2\omega_0$ emission normalized to the laser photon wave vector k_0, i.e., $\tilde{k}_{3/2} = k_{3/2}c/\omega_0$. In the figure only $3/2\omega_0$ wave vectors produced by plasmons propagating downward the density gradient are considered, since they are preferentially detected by the apparatus. Plasmons propagating toward the target produce forward emitted $3/2\omega_0$ photons, which are reflected at their critical surface

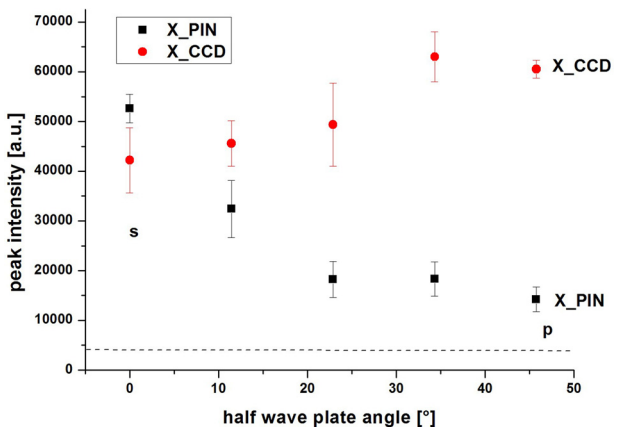

FIG. 6. X-ray yield detected by the PIN diode and CCD vs. the half wave plate angular, changing the laser polarization from S to P.

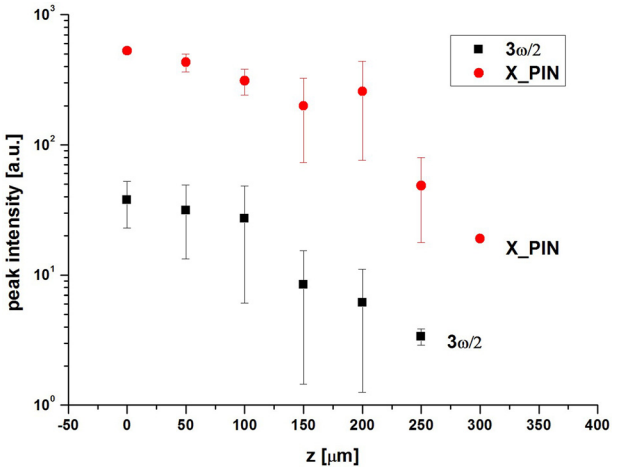

FIG. 7. $3\omega/2$ and X-ray yield (detected from the PIN diode) vs. target position (z axis), with the laser light S-polarized.

and should be in principle taken into account; however, their wave vectors, calculated after reflection at n_c, have a large angle with respect to the collecting optics, and are not considered here. *P*-polarized beam irradiation results in two preferential directions of $3/2\omega_0$ emission, both located in the plane of incidence, produced by the coupling of plasmons with the incoming photons (P_I) and with those reflected at the critical surface (P_R). Their wave vectors at the $n_c/4$ surface form angles α' of 29.4° and 65.6° with respect to the target normal, which become 25.1° and 52° out of the plasma due to light refraction. *S*-polarized beams, conversely, results in two preferential directions of $3/2\omega_0$ emission, produced by the coupling of plasmons with photons reflected at the critical surface. Their wave vectors are symmetrical with respect to the plane $x = 0$ and located at angles $\gamma' = \pm\ 26.3°$ and $\alpha' = 7.3°$ with respect to the planes $x = 0$ and $z = 0$, respectively. After propagation into the plasma, $3/2\omega_0$ photons exit at angles $\gamma = \pm\ 22.6°$ and $\alpha = 6°$. After these calculations, it appears clear that the collecting optics in our set up, located along the laser beam reflection axis, are not far from the expected directions of $3/2\omega_0$ emission obtained for both *P* and *S* polarizations. The wave vectors P_R and S_R shown in the figure, expected for *P* and *S* polarized, respectively, form angles of ~10° and ~ 24° with the axis of signal collection, respectively. According to this analysis, it is also important to remark that the experimental set up preferentially detects the three-halves harmonics signal produced by the coupling of plasmons with the reflected light rather than with incident light. Moreover, the analysis suggests that the different intensity of the $3\omega/2$ signal in P and S polarizations is not due to an experimental bias of the gathering optics, but rather on the fact that S polarized pulses are more strongly reflected at the critical density surface, thus producing a higher three-halves harmonic emission.

Figure 6 shows the behavior of the X-ray yield vs. polarization, measured by the PIN diode and by the CCD, respectively. The emission of the X-rays detected by the PIN has its maximum in S polarization, whereas the CCD reveals the maximum emission in P polarization. Since the two detectors have a similar spectral response, the different behavior is most likely due to the different angle of view of the two detectors, as shown in Fig. 1, where the PIN diode is outside the plane of incidence, while the CCD is in the plane of incidence. The TPD instability grows in both directions, but the laser light polarization influences the fast electrons emission direction. On one hand, the X-ray emission is correlated to the $3\omega/2$ emission. In contrast, X-ray emission in the plane of incidence is well correlated to the 2ω signal, indicating that in this case, X-rays come both from the interaction at the quarter of the critical density and at the critical density itself.

C. 3ω/2 and X-ray vs. target position with S-polarized laser light

From the data presented and preliminarily discussed in the previous paragraphs, it appears quite clearly that in our experiment laser conversion into X-rays involves plasma waves originated by laser coupling with the under-dense region of the pre-plasma. According to the observations reported in the previous paragraph, the S-polarized pulse is strongly reflected at the critical surface, leading to a stronger three halves harmonic emission. In fact a new "focal scan" for X-rays (detected only with PIN-diode) and $3\omega/2$ with S-polarization, was performed to be compared with the one with P-polarization shown in Figs. 2 and 3. The scan was limited to the focal region of spatial range of non vanishing $3\omega/2$ and the result is shown in Fig. 7. The correlation between X-rays emitted outside the incidence plane (in the PIN direction) and $3\omega/2$ emission in the specular direction is confirmed for S-polarization. The ratio between maximum and minimum $3\omega/2$ signals is considerably enhanced here with respect to the P-polarization case. This is a convincing evidence that the plasma scale length at $n_c/4$ is a decisive parameter to identify and control this particular regime of X-ray conversion dominated by the onset of EPW of large amplitude.

IV. DISCUSSION

The experimental data described in the previous section show that, in the presence of a pre-formed plasma, electron plasma waves in the under-dense region, in particular those produced by the TPD process, have a key role in the generation of hard X-rays. The correlation between the X-rays and the 3/2 harmonic emissions and the partial directionality of X-ray emission, which is maximum in the plane of polarization, supports this conclusion. Results also show that the effectiveness of such a mechanism in our conditions lies more on pre-plasma density scale-length than on the intensity of the main pulse. This conclusion has been first inferred from the measurements performed with P-polarized laser light, where both X-rays and 3/2 harmonic emissions are correlated in the focal region of around 500 μm. This behavior is the combined result of both maximum laser intensity I_{main} and maximum pre-plasma density scale length at $n_c/4$, namely $L_{(nc/4)} \approx 4\lambda_0$ at $Z = 0$. However, if we consider the values that laser intensity I_{main} and plasma scale length L take at the boundaries of this range, where $3\omega/2$ emission vanishes, it is clear that the crucial parameter is the scale length of the plasma. In our conditions, $L \approx \lambda_0$ can be taken as the minimum scale length necessary to excite TPD, in agreement with the results reported in Refs. 22–25. At the target position $Z = 250\ \mu$m, where $L \approx \lambda_0$, I_{main} decreases down to $4.5 \cdot 10^{17}$ W/cm^2, which could be still sufficiently intense to excite TPD instability. Indeed, according to the growth rate of TPD calculated[30] in inhomogeneous plasmas, with linear density profile and very long scale length plasma, the threshold of the instability is given by Refs. 6, 12, and 21:

$$\frac{v_{os}^2}{4v_e^2} k_0 L = 0.0504 \frac{L_\mu \lambda_\mu I_{14}}{T} > 3.1, \qquad (1)$$

where v_0 and v_e are the electron quivering and thermal velocities, L_μ and λ_μ are the plasma scale length and the laser wavelength, expressed in μm, T is the plasma temperature expressed in keV. and I_{14} is equal to $I_{main}/10^{14}$ W/cm^2. By considering our experimental parameters and a plasma

temperature of 1 keV, the threshold of TPD given by Eq. (1) is approximately $9{\cdot}10^{15}$ W/cm^2. In the case of relatively short scale-length plasma, as in our experiment, the intensity threshold is expected to increase significantly. Veisz *et al.*[22] found that in experimental conditions similar to ours, the TPD threshold is an order of magnitude larger than that given by Eq. (1). In our experiment, even if we consider a factor 10 of uncertainty, the peak intensity at $\sim$300 μm from the best focus is still much higher than the threshold of TPD. We point out that Stimulated Raman scattering instability may also occur in our conditions. According to Refs. 6 and 15, the SRS threshold is $I_{th} \sim (4{\cdot}10^{17})/\ L(\mu m)\ \lambda\ (\mu m)$ W/cm^2, that leads to the value of $6.4\ {\cdot}10^{17}$ W/cm^2. Tarasevitch *et al.*[23] mentioned the possibility of a sort of a hybrid TPD-SRS instability, assuming that if $\mathbf{k} \approx \mathbf{k}_0$, a combination of SRS and TPD might be excited. In fact, in these conditions, the beating of the electron plasma wave with the pump wave would produce an electromagnetic (SRS) as well as the electrostatic (TPD) response. As TPD, also SRS is expected to generate hot electrons, as shown, for example, in 2D PIC simulations by Quesnel *et al.*[31] Their angular distribution is however expected to peak in the forward direction, since the backscattering SRS growth rate is larger than the side scattering SRS. The contribution of this source of hot electrons, and therefore, of X-ray emission, cannot be separated and quantified by our experimental setup. However, this source is not expected to produce the X-ray anisotropy shown by our measurements, leading us to the conclusion that in our experimental conditions SRS plays a minor role compared to TPD.

These considerations lead to the conclusion that TPD gives a major contribution to the X-ray emission. This balance well explains both the correlation with the $3\omega/2$ emission and the anisotropy in the hard X-rays emission. The growth rate of TPD (γ_0) can be expressed by:[22]

$$\gamma_0 = \frac{\vec{k}_e \vec{v}_{os}}{4} \left| \frac{\left(\vec{k}_e - \vec{k}_0\right)^2 - \vec{k}_e^2}{k_e |\vec{k}_e - \vec{k}_0|} \right|, \qquad (2)$$

where $\mathbf{k}_e$ and $\mathbf{k}_0$ are the wave vectors of the electron waves and of the laser light, and $\mathbf{v}_{os}$ is the electron quivering velocity $= e|\mathbf{E}|/m_e 2\pi\nu$. The scalar product $\mathbf{k}_e\mathbf{v}_{os}$ may explain the behavior reported in Figures 4 and 5. In fact, it is maximum in the plane set by the beam propagation and the polarization axis. According to Eq. (2), in P-polarization the direction of maximum growth of TPD, and therefore, the direction of emission of hot electrons, is close to the CCD angle of view, so that X-rays emission detected by the camera is maximum in p polarization and minimum in s polarization (Figure 6). On the contrary, the PIN diode is placed along the optimal direction of the TPD growth in s polarization (see the trend in Figure 6), so that, an opposite trend of the X-rays yields with laser polarization is expected, as observed. Moreover, we note that the increase of X-ray emission measured in the incidence plane (by the CCD) when polarization changes from S to P—approximately a factor 1.6—is much less than the increase, approximately by a factor 5, measured outside the angle of incidence (by the PIN-X), when the polarization rotates from P to S. These observations provide evidence of anisotropy in the X-ray conversion (in the spectral range we have detected), a clear proof of the strong contribution of electron plasma waves generated by instabilities to the laser energy conversion into X-rays. Previous works already found, separately, a dependence on the laser light polarization of either Kα emission[13,14] or parametric instabilities.[16,17] Such a separation was due to the fact that Kα generation was studied in conditions where the ultrafast laser interaction with the critical density was dominant, while parametric instabilities were considered independently from X-ray conversion efficiency. Here, for the first time, all these phenomena are studied and explained in a unique context. Our observations allow then a real progress in both comprehension of basic physics of ultrafast interaction and improvement of secondary sources efficiency.

A further result, which deserves to be discussed, is the trend of the second harmonic emission, shown in Figures 3(a) and 4. In this context, SH emission is produced by the non-linear interaction of the laser light with plasma waves excited near the critical density and is therefore correlated to the Resonance Absorption mechanism. Combining Maxwell equations, the continuity equation, and the plasma equation of motion, (see Ref. 21 and references therein), the second harmonic current density, which generates the 2nd harmonic radiation, is related to the local electric field by the following:

$$\vec{J}^{(2)}(2\omega) = \frac{in^{(0)}e^3}{4m_e^2\omega^3}\vec{\nabla}(\vec{E}\cdot\vec{E}) + \frac{ie^3}{m_e^2\omega^3}\left(\frac{\vec{\nabla}n^{(0)}\cdot\vec{E}}{1-\omega_p^2/\omega^2}\right)\vec{E}, \quad (3)$$

where $n^{(0)}$ is the unperturbed electron density, $\vec{\nabla}n^{(0)}$ is the longitudinal electron density gradient, ω is the laser angular frequency, and ω_p is the plasma angular frequency. Gizzi *et al.*[21] showed that in the current oscillating at 2ω, the term depending on the gradient of the electron density is dominant and can lead to a considerable enhancement of the electromagnetic field in the region close to critical density layer, thus leading to efficient 2ω generation. According to Fig. 3, the 2ω emission is maximum for P-polarized laser light, which is explained by the vanishing of the second term in Eq. (3) for S-polarized laser light. This can be physically explained by the absence of RA in case of S-polarized light, except for possible minor contributions due to the rippling of the plasma surface, to the aperture of the optics cone. Fig. 3(a) shows that 2ω generation becomes less efficient at best focus, while it exhibits a maximum when the target is shifted by $\sim$300 μm. By looking at the second term in Eq. (3), it is clear that the generation of 2nd harmonic is proportional to $\vec{\nabla}n\cdot\vec{E}$. The density gradient and the electric field, however, have an opposite trend with laser intensity, decreasing and increasing, respectively. Therefore, the maximum 2ω generation is a trade off between these two trends. This condition applies in our experiment at an intensity $I \approx 6.4{\cdot}10^{17}$ W/cm^2, which corresponds to the target positions $z = 200\mu$m. It is worth comparing our results on SH emission to those found in Ref. 21, where 0.8 μm thick plastic foil target were irradiated by a 150 fs FWHM pulse, at an angle of incidence of 20° and an intensity of $5{\cdot}10^{17}$ W/cm^2. The X-ray radiation

was measured by a CCD in the plane of incidence, and the second harmonic radiation was detected in the specular direction, as in our experiment. In Ref. 21, the effect of the preformed plasma was experimentally found to be negligible. The absence of pre-plasma led the authors to consider the RA as the main mechanism of laser absorption and of plasma wave generation. Gizzi *et al.*[21] observed that both X-ray yield and 2ω emission decreased by two orders of magnitude changing the polarization from P to S, although a dip in the 2ω emission was measured for "pure" P-polarization, which they explained as a consequence of wave-breaking. The values reported in Ref. 21 should be compared only with the values reported as "X_CCD" in Fig. 6, because they are referred to a detector in the laser incidence plane. Within this, regarding the correlation between 2ω and X-ray emission, our measurements are in agreement with the measurements of Ref. 21. In addition to that, our new measurements show an important difference, namely the reduction of X-ray emission in the incidence plane when polarization is changed from P to S, with a corresponding increase of X-ray emission in the perpendicular plane. In contrast with Ref. 21, where measurements could be explained invoking RA as the only absorption mechanism, here the interaction in the under-dense plasma is found to compete with interaction at the critical density layers in determining the X-ray emission properties. Given the short scale-length compared to the laser wavelength, Brunel absorption (or *vacuum heating*) effectively describes the regime of absorption that is expected to play a leading role with our steep density profile and relativistic laser intensity. However, possible co-existence of classical RA and vacuum heating with ultra-short laser irradiation of steep critical layers has been proved in Ref. 32.

V. CONCLUSION

The simultaneous detection of X-ray and optical emission during ultra-short, high intensity irradiation of silicon flat samples, by varying pre-plasma scale length and polarization of the laser light, allowed a deeper comprehension of basic physics of ultrafast irradiation of solid samples. The contribution of electron plasma waves (EPW) excited by laser light was proved to play a major role in the X-ray conversion. While with tiny pre-plasma this contribution is mostly generated at the near-critical region, when the pre-plasma increases its scale length up to a few laser wavelength, the contribution of the under-critical region become important. This latter was observed to be even dominant with S-polarized laser light. As a consequence, clear anisotropy in the angular distribution of X-ray emission was also observed, by varying the laser polarization.

The detailed analysis of the experimental data shows for the first time a self-consistent scenario including interaction at the critical density, generation of EPW at $n_c/4$ and hard X-ray generation. In particular, the TPD instability explains very well the directionality of the hot electrons produced both with P and S polarized laser light. We show that this contribution can be optimized by controlling the generation of 3/2 harmonic of the laser light via laser polarization.

Our measurements lead to a unique physical context compared to previous works which studied separately plasma instabilities stimulated by ultra-short laser pulses and X-ray conversion on solid samples, while opening new perspectives for improving non-thermal X-ray plasma sources driven by ultra short laser pulses both in efficiency and directionality.

ACKNOWLEDGMENTS

This work was carried out in the framework of the CNR High Field Photonics Unit (MD.P03.034). The authors acknowledge financial support from the CNR funded Italian research Network "ELI-Italy (Attoseconds)" and from the PRIN project (Contract No. PRIN2012AY5LEL). We also acknowledge contribution from the MIUR-FIRB project "SPARX" (Sorgente Pulsata Auto-Amplificata di Radiazione X) and the INFN "Plasma-med" collaboration. Petra Koester also acknowledges support from the Italian Ministry of Health through the Project No. GR-2009-1608935.

[1]P. Gibbon, *Short Pulse Laser Interaction With Matter: An Introduction* (Imperial College Press, 2005).
[2]D. F. Price, R. M. More, R. S. Walling, G. Guethlein, R. L. Shepherd, R. E. Stewart, and W. E. White, Phys. Rev. Lett. **75**, 252 (1995).
[3]F. Brunel, Phys. Rev. Lett. **59**, 52 (1987).
[4]F. Brunel, Phys. Fluids **31**, 2714 (1988).
[5]J. F. Drake, P. K. Kaw, Y. C. Lee, G. Schmid, C. S. Liu, and M. N. Rosenbluth, Phys. Fluids **17**, 778 (1974).
[6]W. L. Kruer, *The Physics of Laser Plasma Interactions* (Addison-Wesley Publishing Company, 1998).
[7]H. A. Baldis, E. M. Campbell, and W. L. Kruer, *Handbook of Plasma Physics* (Elsevier Science, New York, 1991).
[8]S. J. Karttunen, Laser Particle Beams **3**, 157 (1985).
[9]D. Giulietti, V. Biancalana, D. Batani, A. Giulietti, L. Gizzi, L. Nocera, and E. Schifano, Il Nuovo Cim. D **13**, 845 (1991).
[10]S. Atzeni and J. Meyer-Ter- Vehn, *The Physics of Inertial Fusion* (Oxford Science Publication, 2004).
[11]A. Giulietti, C. Beneduce, T. Ceccotti, D. Giulietti, L. A. Gizzi, and R. Mildren, Laser Particle Beams **16**, 397 (1998).
[12]N. A. Ebrahim, H. A. Baldis, C. Joshi, and R. Benesch, Phys. Rev. Lett. **45**, 1179 (1980).
[13]L. Labate, M. Galimberti, A. Giulietti, D. Giulietti, P. Koester, P. Tomassini, and L. A. Gizzi, Appl. Phys. B **86**, 229, 2007.
[14]M. Chaker, J. C. Kieffer, J. P. Matte, H. Pepin, P. Audebert, P. Maine, D. Strickland, P. Bado, and G. Mourou, Phys. Fluids B **3**, 167 (1991).
[15]B. Soom, H. Chen, Y. Fisher, and D. D. Meyerhofer, J. Appl. Phys. **74**, 5372 (1993).
[16]Ch. Reich, P. Gibbon, I. Uschmann, and E. Forster, Phys. Rev. Lett. **84**, 4846 (2000).
[17]L. M. Chen, P. Forget, S. Fourmax, J. C. Kieffer, A. Krol, C. C. Chamberlain, B. X. Hou, J. Nees, and G. Mourou, Phys. Plasma **11**, 4439 (2004).
[18]T. Mochizuki and C. Yamanaka, Proc. SPIE **0733**, 23 (1986).
[19]R. Kodama, T. Mochizuki, K. A. Tanaka, and C. Yamanaka, Appl. Phys. Lett. **50**, 720 (1987).
[20]A. S. Sandhu, G. R. Kumar, S. Sengupta, A. Das, and P. S. Kaw, Phys. Rev. Lett. **95**, 025005 (2005).
[21]L. A. Gizzi, D. Giulietti, A. Giulietti, P. Audebert, S. Bastiani, J. P. Geindre, and A. Mysyrowicz, Phys. Rev. Lett. **76**, 2278 (1996).
[22]L. Veisz, W. Theobald, T. Feurer, H. Schwoerer, I. Uschmann, O. Renner, and R. Sauerbrey, Phys. Plasma **11**, 3311 (2004).
[23]A. Tarasevitch, C. Dietrich, C. Blome, K. Sokolowski-Tinten, and D. Von der Linde, Phys. Rev. E **68**, 026410 (2003).

[24]C. Li, M. L. Zhou, W.-J. Ding, F. Du, F. Liu, Y.-T. Li, W.-M. Wang, Z.-M. Sheng, J.-L. Ma, L.-M. Chen, X. Lu, Q.-L. Dong, Z.-H. Wang, Z. Lou, S. C. Shi, Z.-Y. Wei, and J. Zhang, Phys. Rev. E **84**, 036405 (2011).
[25]V. Arora, P. A. Naik, J. A. Chakera, R. A. Khan, and P. D. Gupta, Pramana – J. Phys. **75**, 1175 (2010).
[26]L. Veisz, W. Theobald, T. Feurer, H. Schillinger, P. Gibbon, R. Sauerbrey, and M. S. Jovanovic, Phys. Plasma **9**, 3197 (2002).
[27]G. Cristoforetti, A. Anzalone, F. Baffigi, G. Bussolino, G. D'Arrigo, L. Fulgentini, A. Giulietti, P. Koester, L. Labate, S. Tudisco, and L. A. Gizzi, Plasma Phys. Controlled Fusion **56**, 095001 (2014).
[28]L. Labate, A. Giulietti, D. Giulietti, P. Koester, T. Levato, L. A. Gizzi, F. Zamponi, A. Luebcke, T. Kaempfer, I. Uschmann, and E. Foerster, Rev. Sci. Instrum. **78**, 103506 (2007).
[29]G. J. Pert, J. Plasma Phys. **41**, 263 (1989).
[30]A. Simon, R. W. Short, E. A. Williams, and T. Dewandre, Phys. Fluids **26**, 3107 (1983).
[31]B. Quesnel, P. Mora, J. C. Adam, S. Guerin, A. Heron, and G. Laval, Phys. Rev. Lett. **78**, 2132 (1997).
[32]U. Teubner, J. Bergmann, B. van Wonterghem, F. P. Schafer, and R. Sauerbrey, Phys. Rev. Lett. **70**, 794 (1993).